IEEE Access
Multidisciplinary ⋮ Rapid Review ⋮ Open Access Journal

Received 2 February 2023, accepted 13 February 2023, date of publication 2 May 2023, date of current version 5 May 2023.

Digital Object Identifier 10.1109/ACCESS.2023.3260106

RESEARCH ARTICLE

A Low-Complexity Power Maximization Strategy for Coulomb Force Parametric Generators

HAMID MAHBOUBI[1], (Senior Member, IEEE), KAMRAN SAYRAFIAN[2], (Senior Member, IEEE), AND AMIR G. AGHDAM[3], (Fellow, IEEE)

[1]Engineering Division, AECOM, Montreal, QC H2X 3P4, Canada
[2]National Institute of Standards and Technology (NIST), Gaithersburg, MD 20899, USA
[3]Department of Electrical and Computer Engineering, Concordia University, Montréal, QC H3G 1M8, Canada

Corresponding author: Hamid Mahboubi (hamid.mahboubi@aecom.com)

This work was supported by the National Institute of Standard and Technology (NIST) under Grant 60NANB20D163.

This work involved human subjects or animals in its research. Approval of all ethical and experimental procedures and protocols was granted by Concordia University under Application No. 30013664, and NIST under Application No. ITL-2021-0273.

ABSTRACT Energy harvesting (EH) is the process of capturing and storing energy from external sources or the ambient environment. The EH devices have found various emerging applications, particularly, in healthcare sector. Kinetic-based micro energy-harvesting is a promising technology that could prolong the lifetime of batteries in small wearable or implantable devices. In this paper, using a mathematical model of a Coulomb-force parametric generator, we analyze the dependency of the output power on the electrostatic force in this micro-harvester. We propose a low complexity strategy to adaptively change the electrostatic force in order to maximize the harvested power. Simulation results using the human acceleration measurements confirm the effectiveness of the proposed strategy.

INDEX TERMS Micro energy-harvester, wearable sensors, optimization, Coulomb-force parametric generator.

I. INTRODUCTION

Wearable and implantable medical sensors (and actuators) have become a promising interdisciplinary research area in the Internet-of-Things technology for healthcare [1], [2], [3], [4], [5]. With wireless communication capability, these devices will enable an attractive set of applications for remote monitoring of physiological signals such as temperature, respiration, heart rate, glucose, and blood pressure [6], [7]. Increasing functionality and complexity along with the desired miniaturization have drawn the attention of researchers to the limited source of power in these devices [8]. Frequent recharge or battery replacement is simply not feasible in many applications and could negatively impact their market adoption. As such, any technology that can prolong the operational lifetime of these devices will undoubtedly contribute toward their commercial success.

The process of capturing and storing energy from external sources or the ambient environment is referred to as energy harvesting (EH). There are a few sources from which we can harvest energy for wearable or implantable medical sensors. Examples of these sources are ambient light, body heat, and the general movement of the human body [3], [9], [10], [11]. Kinetic energy harvested from the human body motion is the most convenient solution for wearable devices [12], [13], [14]. Authors in [13] designed a low-power kinetic energy harvesting and power management circuit along with a hardware-software context-aware algorithm that reduces quiescent losses and energy storage requirements significantly. As a result, full energy neutrality is allowed even in energy-dry periods. A coaxial wrist-worn energy harvester is proposed in [15] to efficiently capture the biomechanical energy of arm swinging to self-power IoT sensors. The authors used the Lagrangian approach and mirror image method to drive an analytical model for predicting the system dynamics and power generation performance. They also fabricated a miniature prototype containing five pairs of neodymium iron boron magnets and ten series coils to validate the performance of the proposed energy harvester under real walking excitations. In [16], the authors developed

The associate editor coordinating the review of this manuscript and approving it for publication was Eyuphan Bulut.

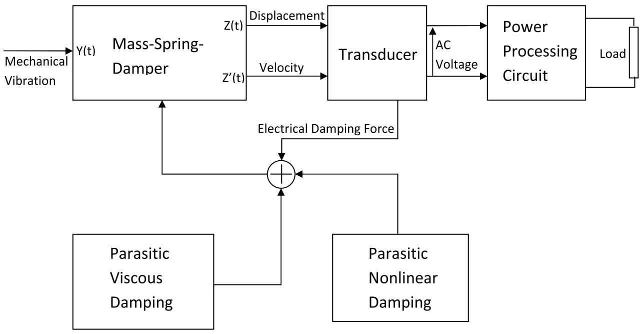

FIGURE 1. Generic electromechanical block diagram of an inertial microgenerator.

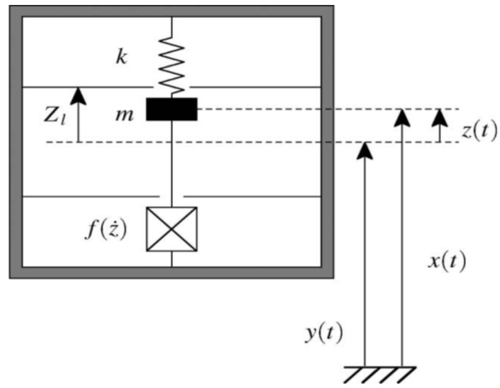

FIGURE 2. Generic model of inertial microgenerator MSD [21].

a closed-form expression for a flexible joint-bending piezoelectric energy harvester placed on the knee joint with relatively low modeling error. The developed model is also validated with a novel piezoelectric energy harvester prototype. A simultaneous energy harvesting and gait recognition architecture has also been developed in [17]. In this architecture, a preprocessing algorithm is proposed to minimize the piezoelectric energy harvester signal distortions caused by energy storage. In addition, a classifier based on long short-term memory (LSTM) deep neural network is proposed in [17] to accurately capture useful information from noisy piezoelectric energy harvester data. In [18], a self-powered health monitoring system has been proposed to collect the movement energy when users walk or run. The proposed system is installed on the shoes and uses a rectifier module to charge the rechargeable lithium battery. Miniaturized energy-harvesting devices, also known as micro-generators, typically consist of a mass-spring-damper (MSD), transducer, and a power-processing circuit, as depicted in Fig. 1 [19], [20]. Movements of the human body are captured by the MSD module and converted into mechanical power. The transducer converts this mechanical power into electrical energy. The power-processing circuitry matches the electrical power generated by the transducer with the load [19], [20].

Kinetic-based microgenerators either utilize the direct application of force on the device or make use of the inertial ambient forces acting on a proof mass. A generic model of an MSD system is shown in Fig. 2 [21]. In this model, the displacement of the mass from its rest position relative to the frame is denoted by $z(t)$. The absolute motion of the frame is $y(t)$ and that of the proof mass is $x(t) = y(t)+z(t)$. The proof mass is able to move between the upper and lower bounds, i.e. $+/- Z_l$, and is attached to a spring-like structure that is denoted with k. Energy is converted when work is done against the transducer's damping force, which opposes the relative motion [21], [22]. The MSD designs that employ a spring (or a spring-like feature) are mainly suitable for applications where the environment causes the system to constantly vibrate [23]. However, the human body motion is typically not a vibrating source of motion. As a result, a microgenerator that can efficiently capture energy from human motion should have a non-resonating design.

One such non-resonating microgenerator architecture is the Coulomb-force parametric generator (CFPG) [21], [22], [24], [25]. The MSD component in this architecture is nonlinear in nature. The proof mass does not vibrate up and down as if anchored on a spring-like structure. Instead, the transducer's damping force, a constant Coulombic electrostatic holding force, keeps the proof mass to an end-stop limit of $+/- Z_l$. The proof mass is held against one end-stop until the external acceleration exceeds the holding force threshold [26]. No power is generated while the proof mass is stuck on either end; instead, power is generated when the proof mass makes a full flight from one end-stop to the other.

Another advantage of the CFPG design is its transduction method. It utilizes electrostatic force rather than making use of electromagnetic or piezoelectric forces. Any of these forces can be used to generate electrical power by converting mechanical energy into an electrical form. However, on the micro-scale, the electrostatic force becomes more significant and suitable for electric power generation [22]. This means that the transduction method in CFPG allows for further miniaturization of the micro-harvester, a highly desirable feature for wearable or implantable sensors.

The authors in [27] highlighted the significant impact of the electrostatic force on the magnitude of the harvested power for various human activities. In [28], an adaptive maximization problem was formulated to exploit the dependency of the optimal holding force on the input acceleration waveform in order to achieve a gain in the micro-generator output power. To the best of our knowledge, the idea of adapting the electrostatic force is relatively new and was first introduced in [29]. Other existing works in the literature related to CFPG do not consider this adaptation possibility for wearable or implant sensors. The authors in [29] investigated several methodologies, such as least square and machine learning to obtain a near-optimal solution to the maximization problem and adapt the electrostatic force based on the acceleration waveform.

Despite the achieved gain in the harvested power, the complexity of the methodologies used in solving the optimization problem is a major concern. High-complexity algorithms would consume more energy, reducing the overall net gain in the generated energy. As such, our objective in this paper is to focus on a low-complexity approach that can be used to adapt the electrostatic force based on the input acceleration. Following an in-depth analysis and observation of the generated power for several artificially generated acceleration waveforms, we propose a computationally simple strategy to efficiently maximize the output power in a CFPG. The complexity of the proposed scheme in this paper is much lower compared to the methodologies proposed in [29]. The results are also verified with actual acceleration measurements from the human body motion.

The remainder of this paper is organized as follows. Section II analyzes the harvested power for step and square acceleration waveforms and highlights the relationships between the input parameters (i.e., amplitude and frequency), the electrostatic holding force, and the instantaneous generated power. In Section III, we propose a low-complexity strategy to adaptively change the electrostatic holding force in order to maximize the average generated power. The performance of the proposed strategy is investigated in Section IV. Finally, conclusions and future plans are discussed in Section V.

II. ANALYSIS OF THE GENERATED POWER FOR SIMPLE INPUT EXCITATIONS

The following nonlinear differential equation captures the dynamics of the MSD module in a CFPG micro energy-harvester [28]:

$$m\ddot{y}(t) = -m\ddot{x}(t) - F(t) \times relay\,(x(t)) \tag{1}$$

In the above equation, m represents the proof mass, $y(t)$ is the motion of the generator frame with respect to the inertial frame, ($\ddot{y}(t)$ is the second derivative of $y(t)$ and indicates the input acceleration), $\ddot{x}(t)$ is the proof mass acceleration, F represents the Coulomb force (also referred to as electrostatic holding force or more generally the MSD's damping force), $x(t)$ is the absolute motion of the proof mass, and $relay(.)$ represents a hysteresis function that switches between $+1$ and -1. The mechanical power generated by the MSD component can be obtained as follows:

$$P(t) = F(t) \times \dot{x}(t) \tag{2}$$

where $F(t)$ is the holding force and $\dot{x}(t)$ represents the velocity of the proof mass.

The Simulink[1] implementation of this model is shown in Fig. 3. The model accurately represents scenarios where the input acceleration does not cause a full end-to-end flight of the proof mass. In those cases, the instantaneous output power will have equal positive and negative components (reactive power); therefore, a zero average power will be generated. This complies with the stated physical requirements in [25].

[1] Simulink is a product of MathWorks, Inc. Simulink has been used in this research to foster research and understanding. Such identification does not imply recommendation or endorsement by the National Institute of Standards and Technology.

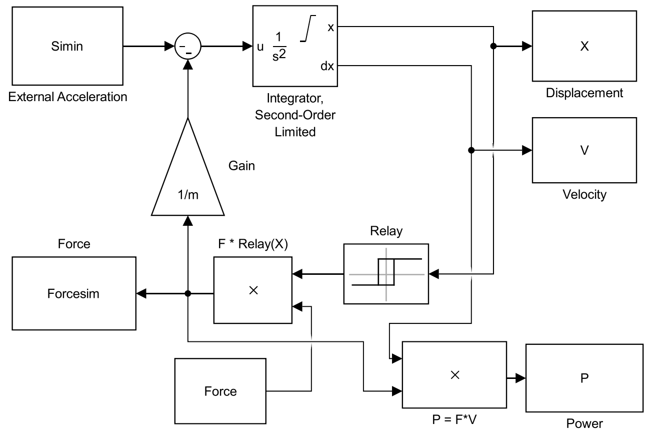

FIGURE 3. Simulink model of CFPG MSD system.

On the other hand, if the amplitude of the input acceleration is sufficient enough to move the proof mass to the other end-point, then positive energy will be generated.

In this section, using the Simulink model of the MSD, we study the average generated power for simple acceleration waveforms such as step function, square and sinusoidal waves. One important objective here is to underline the significant impact of the electrostatic force F on the generated power. The results in this paper have been obtained assuming an MSD with the following specifications: proof mass = 0.965 g, and the distance between the two end-stops = 5 mm. We conjecture that the general conclusions expressed here are independent of the MSD specifications.

A. STEP FUNCTION

Consider a step function with an amplitude 4 m/s^2 as the input acceleration waveform to a CFPG. The total duration of the waveform is assumed to be 10 seconds. Fig. 4 demonstrates the impact of the electrostatic force on the output mechanical power from the MSD module. As observed, the average generated power increases monotonically by increasing the electrostatic force up to a certain threshold and then drops to zero. This threshold changes by changing the amplitude of the step function. Let the optimal electrostatic force for the step function with amplitude a be denoted by $F_{opt}(au(t))$. In general, this optimal value is a linear function of the amplitude of the step function, as shown in Fig. 5. Therefore, we will have $F_{opt}(au(t)) = G(|a|)u(t)$, where $G(.)$ represents the linear function noted above, and $|.|$ represents the absolute value function. For the example in Fig. 4, we have $F_{opt}(4u(t)) = 3.85u(t)$ mN. Choosing this function for the holding force will yield maximum power for a given step function.

B. SQUARE WAVE

Consider a square wave as the acceleration input to a CFPG. The amplitude and duration of the square wave are also assumed to be 5 m/s^2 and 10 seconds, respectively. The main harmonic frequency of the square wave (hereafter simply referred to as frequency) is considered to be 1 Hz. In this

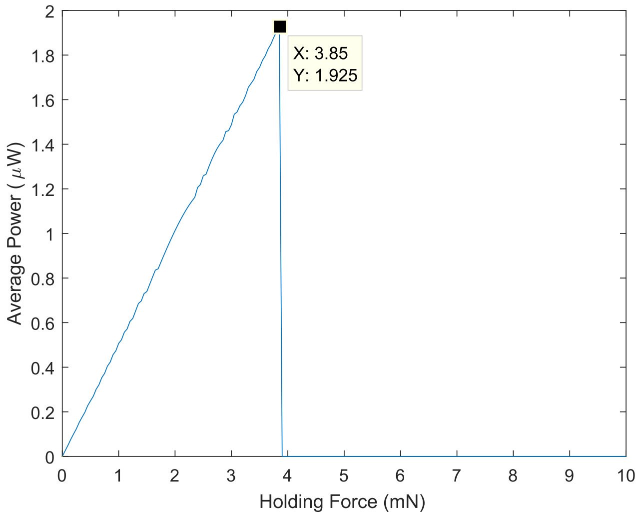

FIGURE 4. Average power vs holding force for step function with amplitude 4 m/s^2.

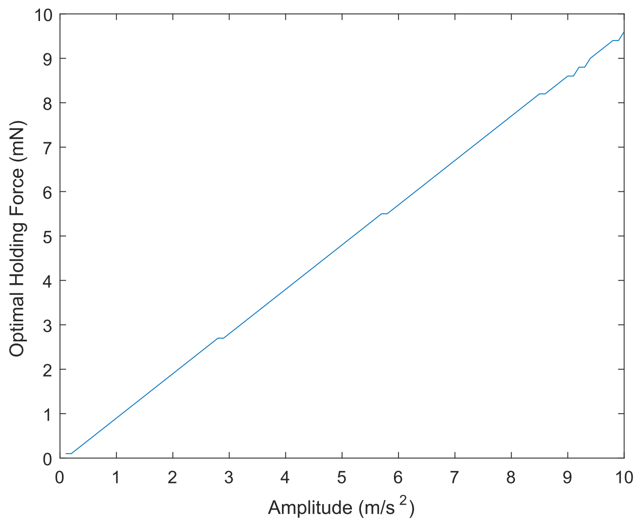

FIGURE 5. Optimal value of holding force for a step function with varying amplitude.

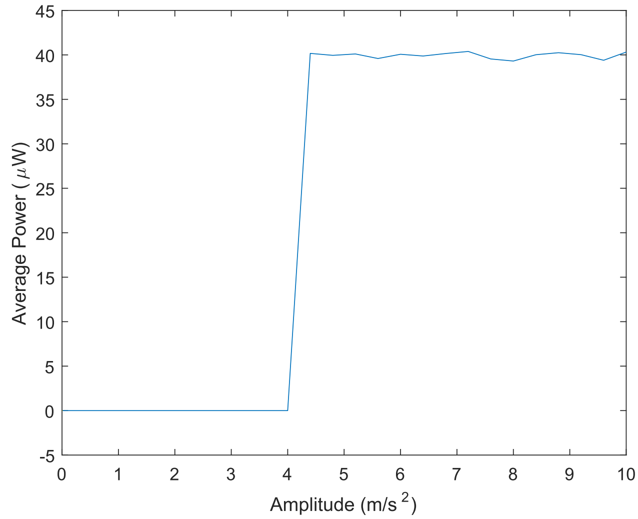

FIGURE 6. Average power vs acceleration amplitude for acceleration input frequency = 1 Hz and holding force = 4 mN.

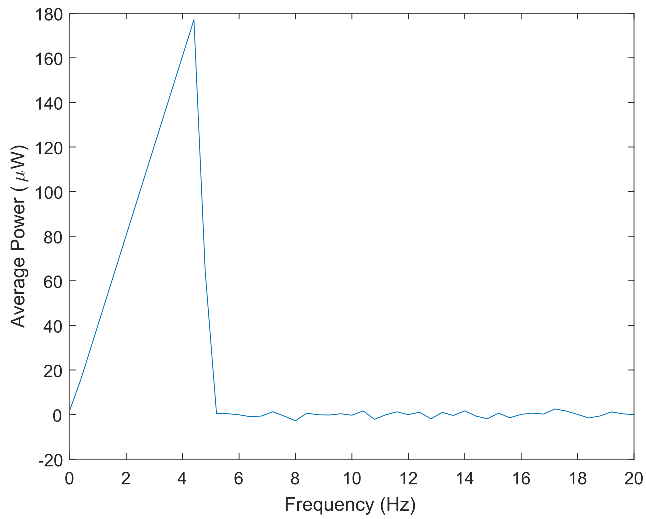

FIGURE 7. Average power vs acceleration frequency for holding force = 4 mN and acceleration input amplitude = 5 m/s^2.

subsection, we study the impact of the frequency, amplitude, and holding force on the generated power for this input acceleration waveform. Fig. 6 displays the average output power versus input amplitude when the frequency is kept constant and $F = 4$ mN. As observed, there exists a threshold for the input amplitude, below which there is no generated power. However, above that threshold, the amount of the average generated power is constant. A similar characteristic can also be observed for other combinations of constant frequency and holding force. This behavior is expected since, for weak input excitations (i.e. low amplitudes), the holding force will prevent the proof mass from moving. At some point, the input acceleration overcomes the holding force, and the proof mass would be able to oscillate freely between the frame endpoints, hence, generating power. The constant value of the generated power is due to the constant frequency of the square wave.

Fig. 7 displays the average output power versus frequency when the input acceleration amplitude is kept constant and holding force = 4 mN. The average generated power monotonically increases with increasing frequency up to a certain value, after which it drops to zero. Higher frequencies translate to a faster oscillation of the proof mass, resulting in higher generated power. However, beyond a certain value, the frequency would be too high for the proof mass to make complete end-to-end flights, and as a result, no power will be generated.

Next, we investigate the effect of the electrostatic force on the average power when the square wave amplitude and frequency are kept constant. Fig. 8 displays the average output power versus F when the amplitude is 5 m/s^2 and the

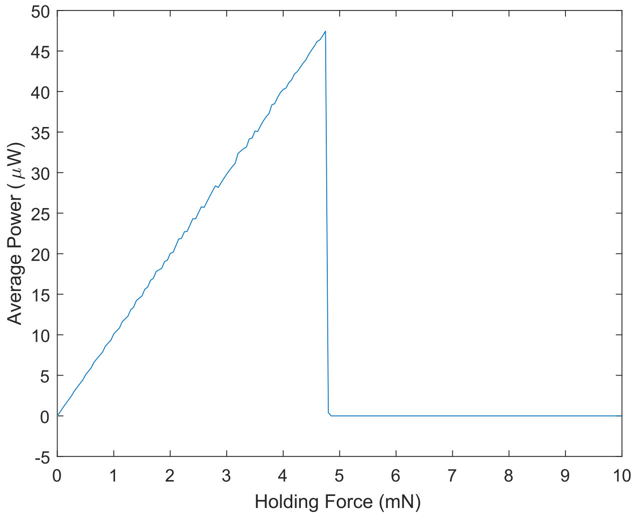

FIGURE 8. Average power vs holding force for square wave with frequency = 1 Hz and amplitude = 5 m/s^2.

frequency is 1 Hz. As observed, the average power increases linearly with F but drops to zero beyond a certain value. The peak average power in this example is 47.44 μW. An electrostatic force stronger than this value will simply prevent the proof mass from moving, resulting in zero output power [25]. This behavior also occurs regardless of the specific values of the amplitude and frequency of the input acceleration.

The results in Fig. 8 also point to the existence of an optimal value for the electrostatic force F for any given square wave excitation. This observation is highlighted in Fig. 9, where the optimal value of F for a given input acceleration frequency and amplitude is displayed. The maximal amount of the generated average power corresponding to these optimal values is shown in Fig. 10. The existence of an optimal value for F and its dependency on the characteristics of the acceleration waveform confirm that the holding force can be a design parameter in a CFPG device [28]. By carefully adapting F to the variations of the input acceleration, the energy harvesting capability of the device can be greatly improved.

C. SINUSOIDAL WAVE

Now consider an acceleration input in the following form:

$$y(t) = \begin{cases} 6\mathrm{Sin}(6\pi t) & 0 \leq t < 5 \\ 3\mathrm{Sin}(4\pi t) & 5 \leq t \leq 10 \end{cases} \tag{3}$$

Fig. 11 depicts the average generated power versus different values of the holding force. As observed, the average generated power increases by increasing the holding force up to 2.2 mN, then sharply drops and again increases by increasing the electrostatic force up to 4.3 mN. The average power sharply drops to zero after increasing the holding force beyond 4.3 mN. At that point, the holding force becomes too strong, preventing the proof mass from moving, and hence, resulting in zero output power.

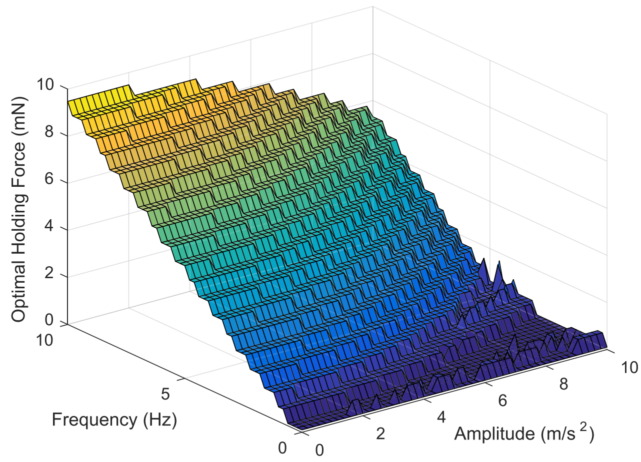

FIGURE 9. Optimal value of holding force for square input with varying amplitude and frequency.

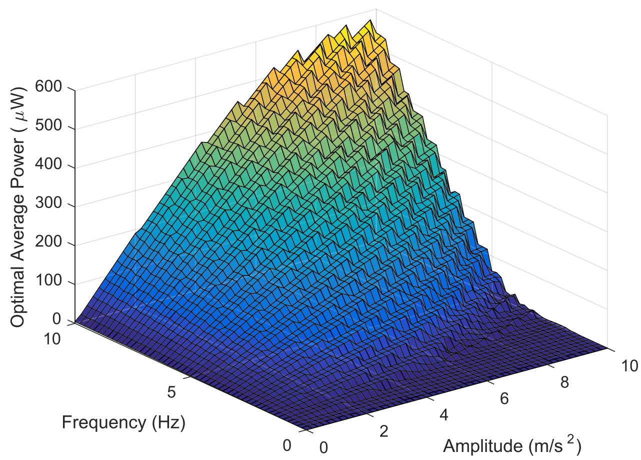

FIGURE 10. Optimal average power for square input with varying amplitude and frequency.

Fig. 12 shows the proof mass position and generated power when the holding force is equal to 2.2 mN. Since the holding force is not too large, the proof mass can make a full flight in both time intervals [0, 5) and [5, 10], where the amplitude of the sinusoidal input is 6 m/s^2 and 3 m/s^2, respectively. Therefore, power is generated in both time intervals [0, 5) and [5, 10] when $F = 2.2$ mN.

By increasing holding force beyond 2.2 mN, the generated power in the time interval [0, 5) increases; however, the proof mass cannot make a full flight during the time interval [5, 10]. The generated power and proof mass position for the constant optimal holding force $F = 4.3$ mN is shown in Fig. 13. Although the proof mass cannot move during the time interval [5, 10], the generated power in the time interval [0, 5) is large enough to make $F = 4.3$ mN the optimal constant holding force for the entire interval [0, 10].

Figs. 12 and 13 again demonstrate how judicious adaptation of F to variations in input acceleration can result in higher average harvested power. In this example, choosing

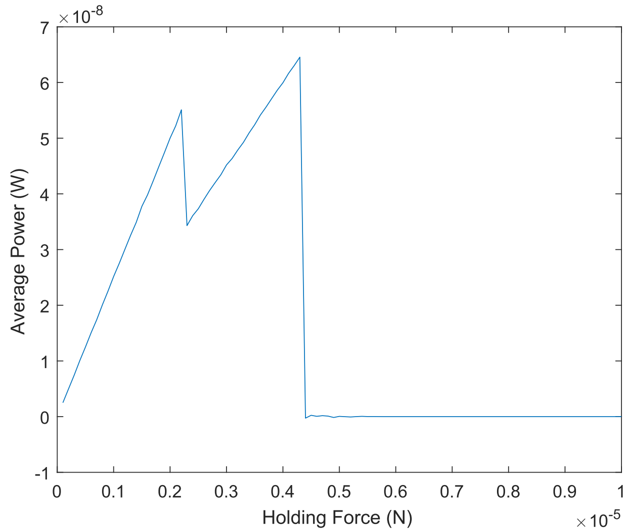

FIGURE 11. Average power vs holding force for acceleration input given in Eq. (3).

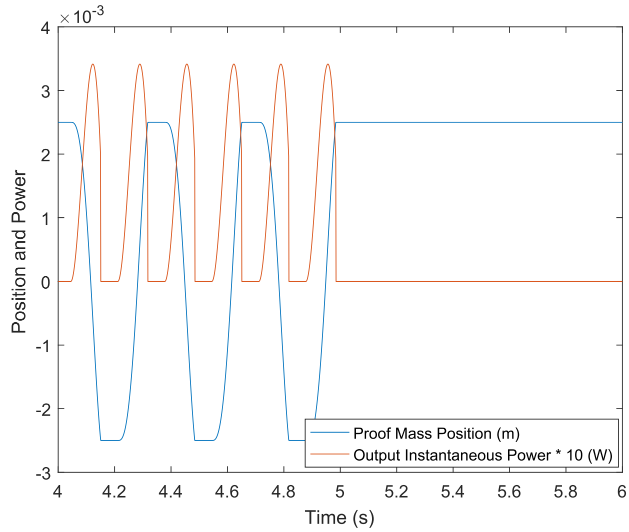

FIGURE 13. Generated power and proof mass position for acceleration input given in Eq. (3) when holding force is optimal (i.e., $F = 4.3$ mN).

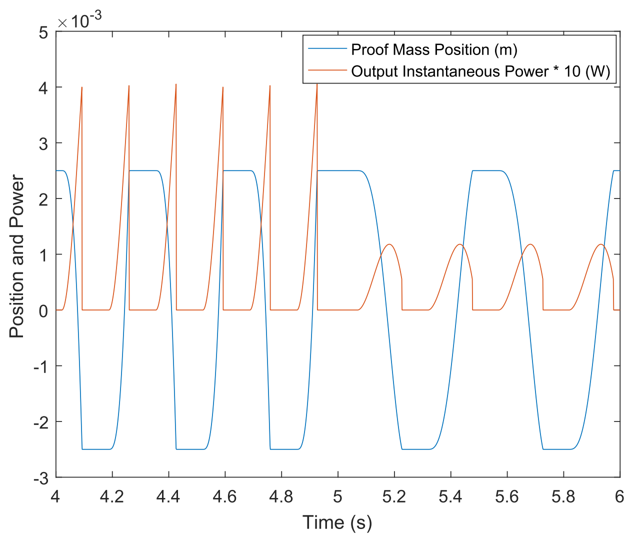

FIGURE 12. Generated power and proof mass position for acceleration input given in Eq. (3) when $F = 2.2$ mN.

$F = 4.3$ mN and $F = 2.2$ mN for the time intervals $[0, 5)$ and $[5, 10]$, respectively, results in higher output power compared to the case when an optimal constant electrostatic force is used for the entire duration of the input waveform (i.e. $[0, 10]$.

The examples provided in this section not only provide some valuable insight into the impact of the electrostatic force, as well as the acceleration waveform amplitude and frequency on the harvested power, but they also lead us to an intuitive and simple scheme to adapt F in a CFPG device. Since any acceleration waveform can be approximated by a sequence of weighted and delayed step functions, in the next section, we propose a low-complexity methodology to adaptively change the holding force based on the input acceleration waveform.

III. A LOW COMPLEXITY ADAPTIVE STRATEGY

In this section, we develop a strategy to adaptively adjust the electrostatic force such that the generated power increases. Consider the acceleration waveform $y(t)$ during the time interval $[0, T]$. Divide this time interval into n equal subintervals of length δ, i.e., $[k\delta, (k+1)\delta]$, $k \in \mathbf{n} := \{0, 1, \ldots, n-1\}$. We assume that there is the capability to adjust the electrostatic force at the beginning of each subinterval in order to maximize the average output power of the MSD. Let F_k denote the constant value of the electrostatic force during the time interval $[k\delta, (k+1)\delta]$. As indicated in Eq. (2), the output power during this time interval is directly proportional to F_k. Therefore, the power maximization problem can be formulated as follows:

$$\underset{F_0,F_1,\ldots,F_{n-1},\delta}{\operatorname{argmax}} \left[\frac{1}{T} \sum_{k=0}^{n-1} \int_{k\delta}^{(k+1)\delta} F_k \times \dot{x}(t)dt \right] \tag{4}$$

where δ and F_k, $k = 0, 1, \ldots, n-1$, are design parameters, and $\dot{x}(t)$ represents the velocity of the proof mass. The inequalities $F_k \geq 0$ and $\delta > 0$ are the constraints of the above-mentioned optimization problem. Aside from an exhaustive search, identifying a methodology that can determine the optimal values δ^* and F_k^* in Eq. (4) is quite challenging. In this paper, we first simplify the problem by assuming that δ is a given constant. Then, using our observations with the simple acceleration waveform discussed in the previous section, we propose a low-complexity methodology that can serve as an approximate solution to Eq. (4). To this end, we first approximate the input acceleration $y(t)$ with the waveform $\widetilde{y}(t)$ as a summation of weighted and delayed step functions. Define y_k as the input acceleration $y(t)$ at $t = k\delta$. Then, we will have:

$$y(t) \approx \widetilde{y}(t) = \sum_{k=0}^{n-1} y_k[u(t - k\delta) - u(t - (k+1)\delta)] \tag{5}$$

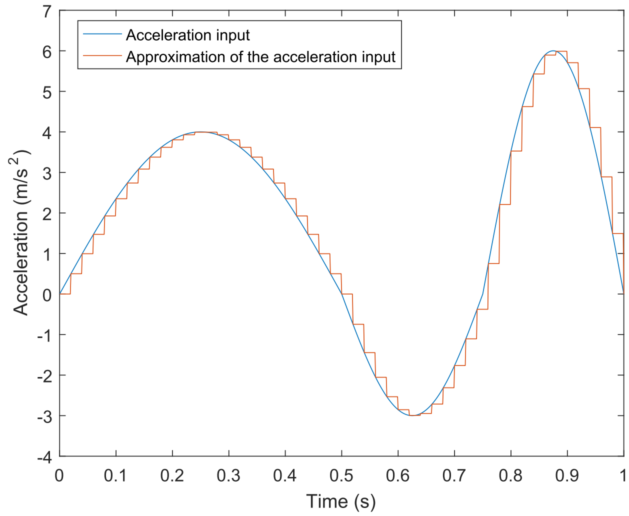

FIGURE 14. Acceleration waveform and its approximation.

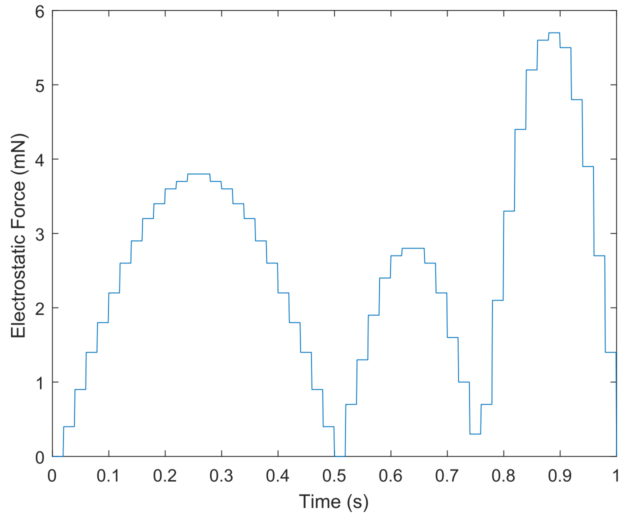

FIGURE 15. Adaptive electrostatic force corresponding to acceleration input $y(t)$ given in Fig. 14.

Fig. 14 demonstrates a sample acceleration waveform and its approximation according to Eq. (5) with $\delta = 0.02$ s.

With $\widetilde{y}(t)$ expressed as a sequence of weighted step functions, we can use the results obtained in Section II to estimate the optimal value for the electrostatic force as follows:

$$F_{opt}(\widetilde{y}(t)) = F_{opt}(\sum_{k=0}^{n-1} y_k[u(t-k\delta) - u(t-(k+1)\delta)] \quad (6)$$

Eq. (6) can be further simplified to:

$$F_{opt}(\widetilde{y}(t)) \approx \sum_{k=0}^{n-1} G(|y_k|)[u(t-k\delta) - u(t-(k+1)\delta)] \quad (7)$$

Note that the results for a single step function assumed that the proof mass is initially resting at an end-stop. Here, we propose to use Eq. (7) as an approximate solution to the maximization problem expressed by Eq. (4). In other words, if F_k^{adp} denotes an adaptive strategy to update the value of F_k at each time instant $k\delta$, $k \in \mathbf{n}$, then we claim that the following equation:

$$F_k^{adp} = G(|y_k|) \quad (8)$$

provides a low complexity scheme to adjust the electrostatic force for input acceleration waveform $y(t)$ at each time instant $k\delta$, $k \in \mathbf{n}$. Fig. 15 demonstrates the adaptive electrostatic force based on Eq. (8) corresponding to the input waveform shown in Fig. 14.

The flowchart in Fig. 16 describes the details of the proposed strategy. In this flowchart, H^* represents the solution of Eq. (4), and δ^* is the optimal value of the adaptation interval.

Remark 1: When $\delta = T$, solving the maximization problem in Eq. (4) results in the optimal constant value for the electrostatic force, hereafter denoted by F^c_{opt}. It is to be noted that finding F^c_{opt} is not realistic, as in most practical situations, knowledge of the entire waveform is not available or predictable beforehand. In the next section, we compare

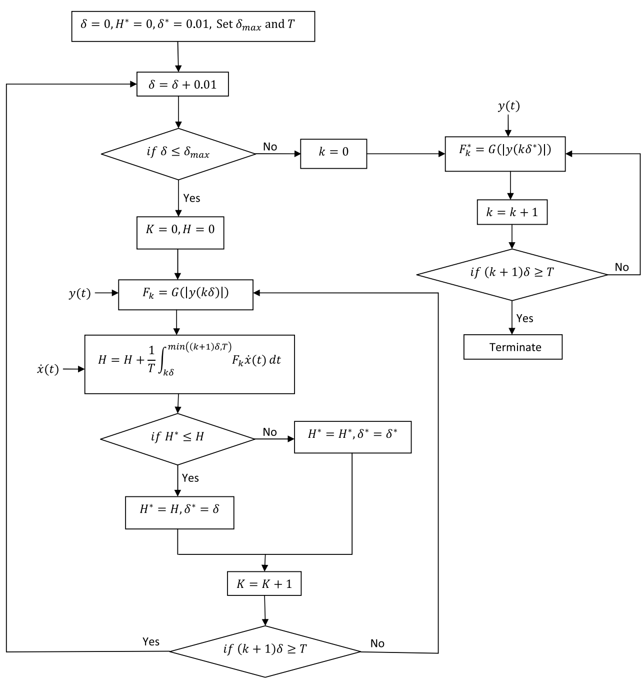

FIGURE 16. Flowchart of the proposed method.

the harvested power under our proposed adaptive scheme with several constant values of the electrostatic force F^c. We have also considered F^c_{opt} for performance evaluation purposes, although obtaining its value is not practically feasible. In general, the gain of any adaptive scheme should be measured against a constant electrostatic force which may not necessarily be optimal.

IV. SIMULATION RESULTS

In this section, the effectiveness of the proposed adaptive strategy is investigated using acceleration data measured from several human activities.[2] The data is obtained by using an X16-mini USB triaxial accelerometer.[3] Note that, in practice, the micro-harvester will be integrated with a wearable or implantable sensor. Usually, the location of the sensor on the human body is not a design parameter, and is mainly determined by the nature of the sensing application. With a small dimension of 51×25×13 mm, this accelerometer can be easily placed on different parts of the body to perform various measurements. The measurement samples are time-stamped and stored in a CSV file in an onboard memory for later retrieval. Although the frequency of typical human motion is typically less than 5 Hz, note that some actions like heel strike and muscle vibration with a sudden movement could produce higher frequency acceleration on the device that is attached to the surface of the body. The accelerometer has adjustable sampling rates from 12 Hz to 800 Hz. A sampling rate of 100 Hz has been used in our measurements.

Extensive experiments using this accelerometer have been done to generate a dataset of various acceleration waveforms corresponding to several human activities at various intensity levels and different placements of the accelerometer. Note that if the final sensor position is known, the optimum orientation of the micro-harvester inside the sensor should be along the direction of the most body movement, i.e., the highest acceleration.

Example 1: Fig. 17 shows a sample 100-second acceleration waveform during light jogging with the accelerometer located on an individual's wrist. Given the description under Remark 1, and assuming $\delta = T = 100$ s, we obtain the optimal value of the constant electrostatic force to be $F^c_{opt} = 3.5$ mN. As mentioned earlier, this value is obtained through an exhaustive search and assuming that the knowledge of the entire acceleration waveform is known to the micro-harvester. Using Eq. (8), we can also determine the sequence of adaptive electrostatic force F^{adp}_k, $k = 0, 1, 2, \ldots, 5000$ when $\delta = 0.02$ s.

Figs. 18 and 19 display the instantaneous power generated under the adaptive strategy and optimal constant holding force, respectively. There are two observations when comparing these figures. First, the number and intensity of negative spikes are far less using the adaptive strategy. As described earlier, these spikes are due to incomplete flights by the proof mass, resulting in no generated power. Second (although this may not be quite visible), there are also far fewer instances of zero instantaneous power with the adaptive strategy. These instances correspond to conditions when the proof mass cannot move due to excessive holding force. The combination of these two observations translates to higher average power under the adaptive strategy compared to the optimal constant

[2]The experiments were conducted according to the research ethics regulations under the approval number 30013664 at Concordia University and ITL-2021-0273 at NIST.

[3]X16 mini accelerometer is a product of Gulf Coast Data Concepts, LLC. Commercial products mentioned in this paper are merely intended to foster research and understanding. Such identification does not imply recommendation or endorsement by the National Institute of Standards and Technology.

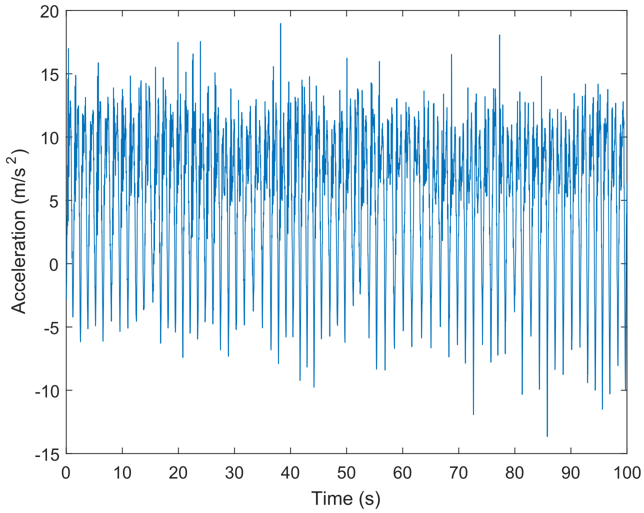

FIGURE 17. Acceleration waveform resulting from jogging with the accelerometer on the wrist.

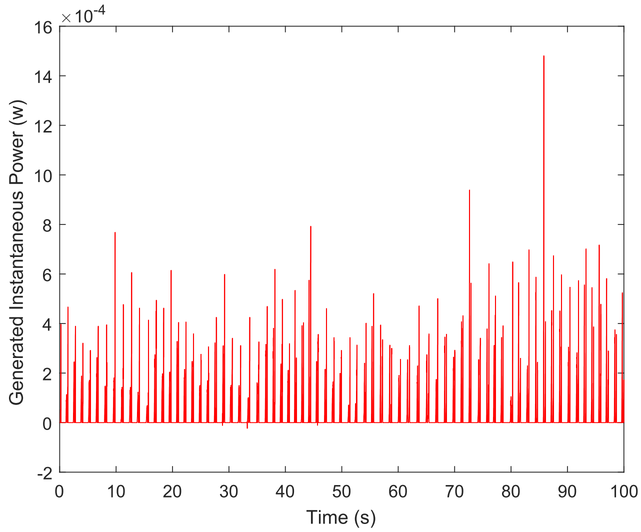

FIGURE 18. Instantaneous output power under the adaptive holding force strategy.

holding force, even though the optimal constant force cannot be realistically obtained in practical scenarios. The numerical accuracy of the generated power, harvested energy, and electrostatic force are 0.01 μW, 0.1 μJ, and 0.1 mN, respectively.

The performance of the adaptive strategy should also be compared with that of the non-optimal constant holding force to determine the more realistic gain of the strategy. For this purpose, we also consider two other values of constant electrostatic force to evaluate the energy harvesting capability of the CFPG with our proposed adaptive scheme. Fig. 20 shows the output energy of the MSD unit with constant holding forces $F^c = 2$ mN, $F^c = 4.5$ mN, the optimal constant force $F^c_{opt} = 3.5$ mN, and the proposed adaptive force. As observed, the harvested energy under the adaptive scheme is considerably higher compared to all cases with a constant holding force. Even compared to the practically unobtainable

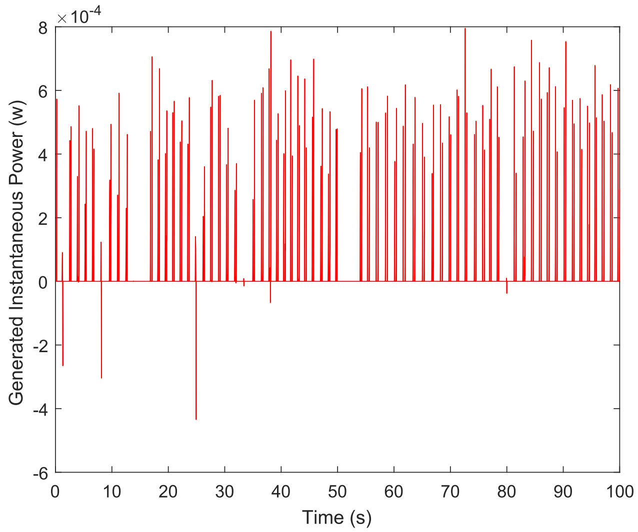

FIGURE 19. Instantaneous output power under the optimal constant electrostatic force.

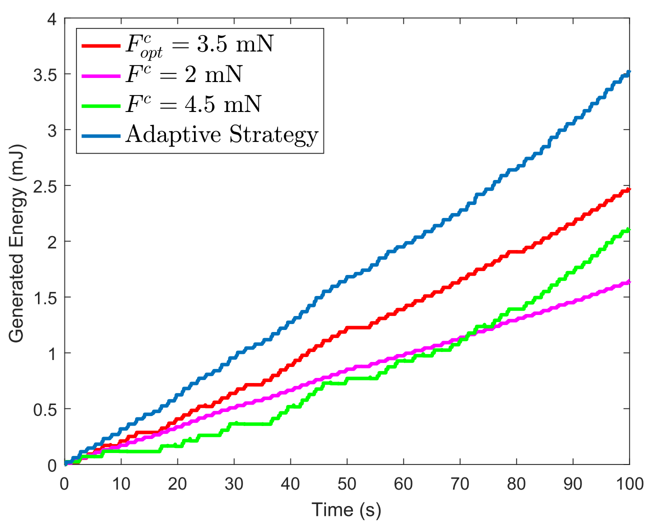

FIGURE 20. Harvested energy under the adaptive holding force strategy, optimal constant electrostatic force, $F^c = 2$ mN and $F^c = 4.5$ mN.

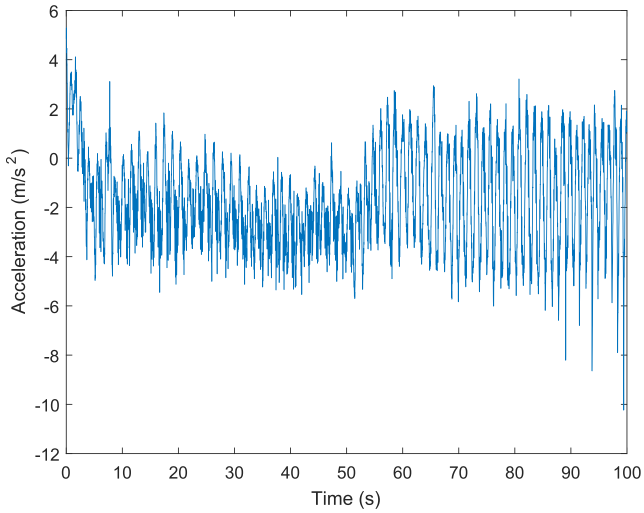

FIGURE 21. Acceleration waveform corresponding to random body movements with the accelerometer placed on the chest.

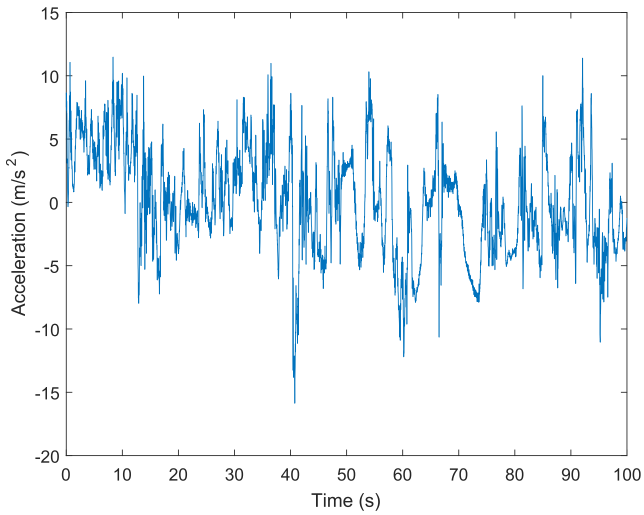

FIGURE 22. Acceleration waveform corresponding to random body movements with the accelerometer placed on the wrist.

optimal constant force (F^c_{opt}), a gain of 42% can be achieved by using our proposed strategy for the light jogging example waveform.

Example 2: Figs. 21 and 22 show the acceleration waveforms for random body movements when the accelerometer is placed on the chest and wrist, respectively. The optimal constant electrostatic force for these waveforms are $F^c_{opt} = 1$ mN and $F^c_{opt} = 2.9$ mN, respectively. Considering an adaptation interval of $\delta = 0.02$, Figs. 23 and 24 display the harvested energy under the adaptive holding force strategy, the optimal constant force and constant forces $F^c = 0.5$ mN, $F^c = 1.5$ mN. As observed, the harvested energy with the acceleration data from the chest is 652.0 μJ, 263.7 μJ, 211.8 μJ and 141.2 μJ under the adaptive strategy, optimal constant holding force, and constant forces $F^c = 0.5$ mN and $F^c = 1.5$ mN respectively. This indicates 147%, 207%, and 362% increases in the harvested energy using the proposed adaptive strategy compared to the harvested energy using optimal constant force, constant forces $F^c = 0.5$ mN and $F^c = 1.5$ mN, respectively. Similarly, with the acceleration data obtained from the wrist motion, the harvested energy under the adaptive strategy is 790.9 μJ, 24%, 212%, and 65% more than the 635.5 μJ, 253.3 μJ, and 480.5 μJ harvested under the optimal constant electrostatic forces $F^c = 0.5$ mN and $F^c = 1.5$ mN, respectively. These results indicate a noticeable gain in our proposed adaptive strategy for the harvested energy from the kinetic motion of the human body.

Figs. 25 and 26 display the instantaneous power generated under the adaptive strategy and optimal constant holding force for the chest acceleration data. Similar to the results for the light jogging motion, there are fewer instances of zero instantaneous power with the adaptive strategy. In addition,

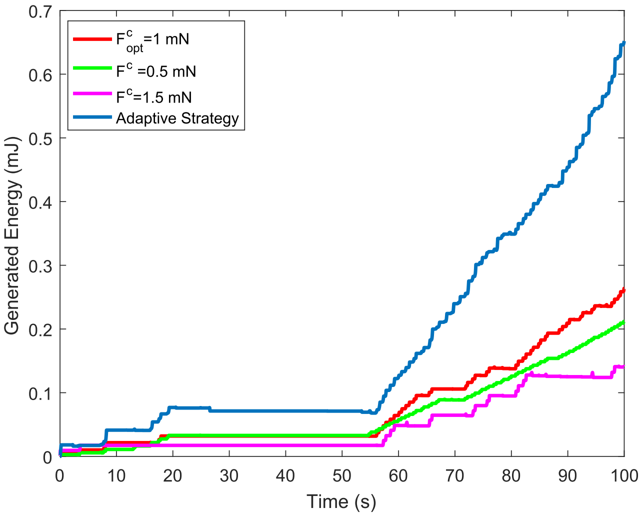

FIGURE 23. Harvested energy under the adaptive holding force strategy, optimal constant electrostatic force, $F^c = 0.5$ mN and $F^c = 1.5$ mN with the acceleration data from the chest.

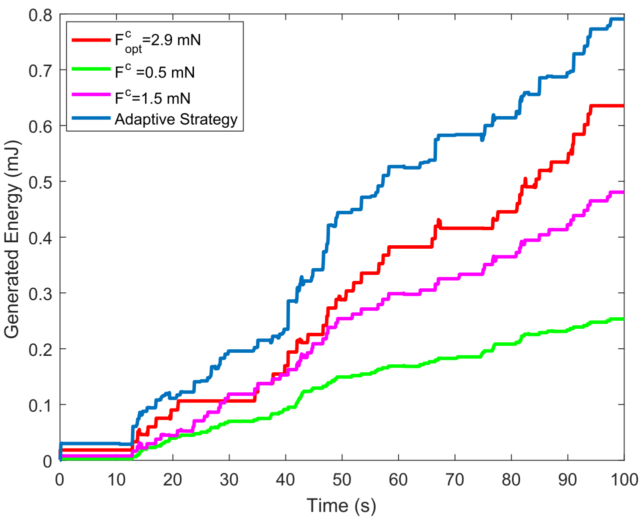

FIGURE 24. Harvested energy under the adaptive holding force strategy, optimal constant electrostatic force, $F^c = 0.5$ mN and $F^c = 1.5$ mN with the acceleration data from the wrist.

the generated instantaneous power with the adaptive strategy is visibly higher than when constant holding force is used. As a result, higher average power under the adaptive strategy is obtained.

Remark 2: Note that the X16-mini triaxial accelerometer measures the acceleration in all three x, y, and z directions. These directions are relative to the accelerometer and are not according to a universal body coordinate system. The average generated power in different directions depends on the placement of the accelerometer and the intensity of the human activity. Table 1 shows the average generated power corresponding to several human activities at various intensity levels and different placements of the accelerometer. In this table, $P_x^{avg}(F_\delta^{adp})$, $P_y^{avg}(F_\delta^{adp})$ and $P_z^{avg}(F_\delta^{adp})$ represent the average generated power in directions x, y and z, respectively.

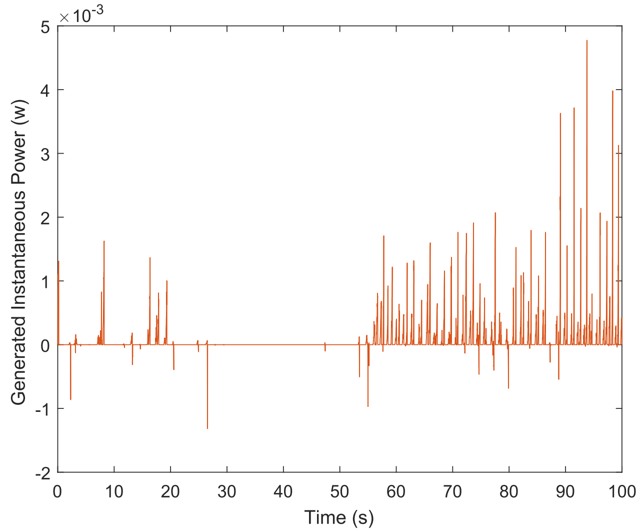

FIGURE 25. Instantaneous output power under the adaptive holding force strategy with acceleration waveform from the chest.

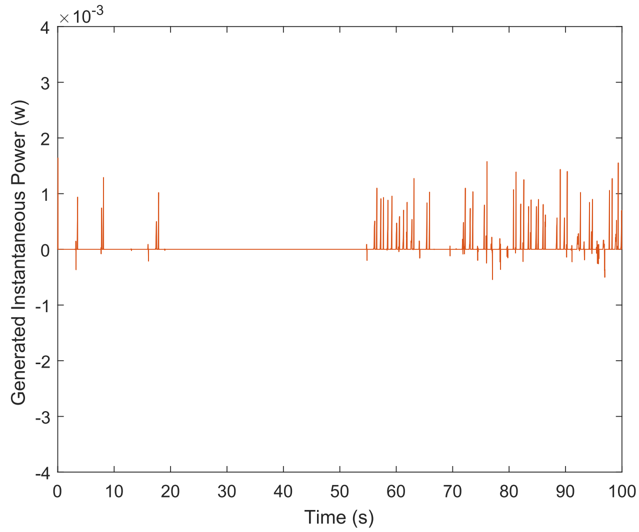

FIGURE 26. Instantaneous output power under the optimal constant electrostatic force with acceleration waveform from the chest.

A. IMPACT OF THE ADAPTATION INTERVAL

As mentioned in Section III, the adaptation interval δ is a design parameter and should be chosen properly. Using the acceleration waveform shown in Fig. 21, Fig. 27 displays the average generated power for different values of δ under the adaptive holding force strategy. Fig. 28 demonstrates the average generated power for different values of the constant electrostatic forces. Comparing these results indicates that for adaptation intervals less than $\delta \approx 0.2$ s, the average generated power under the adaptive strategy is more than when the optimal constant electrostatic force is used.

To further investigate the impact of the adaptation interval δ on the average generated power and gain some insight into the proper values for δ, extensive simulations on acceleration waveforms obtained from different human activities

TABLE 1. Average generated power in x, y, and z directions for different activities.

Body Part	Activity	Level	$P_x^{avg}(F_\delta^{adp})$ (μW)	$P_y^{avg}(F_\delta^{adp})$ (μW)	$P_z^{avg}(F_\delta^{adp})$ (μW)
Arm	sit-ups	slow	0.40	0.21	5.79
Arm	sit-ups	medium	0.37	0.42	8.42
Arm	sit-ups	intense	0.87	0.11	11.00
Arm	jogging	slow	0.36	0.16	3.87
Arm	jogging	medium	0.38	0.75	7.38
Arm	jogging	intense	0.29	0.10	17.70
Leg	sit-ups	slow	1.34	0.82	4.19
Leg	sit-ups	medium	0.49	2.47	5.83
Leg	sit-ups	intense	0.33	2.72	9.95
Leg	jogging	slow	0.38	4.20	15.80
Leg	jogging	medium	0.35	9.97	26.50
Leg	jogging	intense	0.16	45.1	64.4
Chest	sit-ups	slow	0.43	2.05	10.20
Chest	sit-ups	medium	0.45	2.50	14.00
Chest	sit-ups	intense	0.40	5.84	18.20
Chest	jogging	slow	0.47	3.08	0.49
Chest	jogging	medium	0.41	1.94	0.60
Chest	jogging	intense	4.05	5.52	15.40
Wrist	sit-ups	slow	0.33	0.19	1.69
Wrist	sit-ups	medium	1.15	0.51	2.79
Wrist	sit-ups	intense	1.02	0.26	5.72
Wrist	jogging	slow	8.09	0.13	1.89
Wrist	jogging	medium	17.10	0.12	11.30
Wrist	jogging	intense	44.50	0.19	50.10

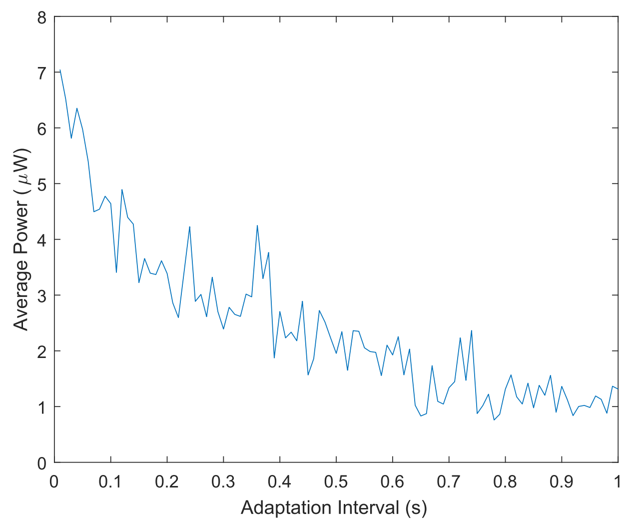

FIGURE 27. Average generated power vs adaptation interval δ under adaptive holding force strategy for random body movements of Fig. 21.

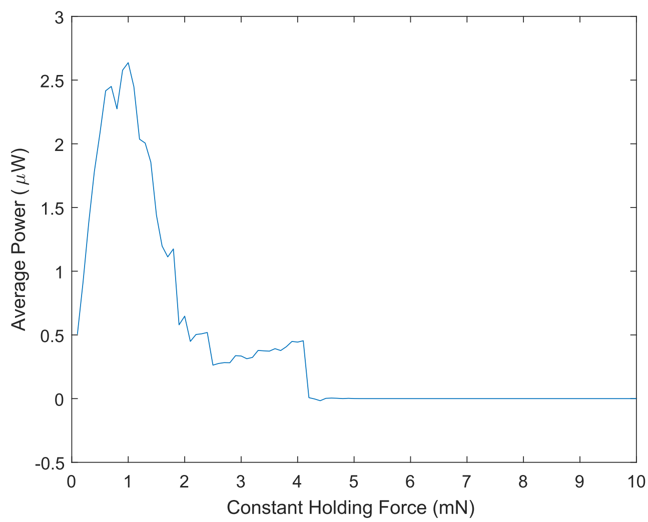

FIGURE 28. Average generated power for different constant electrostatic forces for random body movements of Fig. 21.

have been performed. Acceleration data were collected for sit-ups and jogging from a volunteer who was wearing the accelerometer on his arm, leg, chest, and wrist for several minutes. To consider the changes in amplitude and frequency of the acceleration waveform, data for each activity was collected with different intensity levels, i.e., slow, moderate and intense. We applied the adaptive strategy to the collected data for different values of δ ranging from 0.01 s to 1 s (with the step size of 0.01 s) and compared its performance with the optimal constant holding force. Assuming an adaptation interval of size δ, let the piecewise constant electrostatic force under the adaptive strategy be denoted by F_δ^{adp}.

TABLE 2. Optimal adaptation interval and optimal average generated power for different activities.

Body Part	Activity	Level	$[\delta]^*$ (s)	δ^* (s)	$P(F_{\delta^*}^{adp})$ (μW)	$P(F_{opt}^{c})$ (μW)	$PI_{F_{opt}^c}^{adp,\delta^*}$	$PI_{F_1^c}^{adp,\delta^*}$	$PI_{F_2^c}^{adp,\delta^*}$
Arm	sit-ups	slow	[0.01,0.09]	0.01	10.46	6.69	56.3%	158.9%	547.7%
Arm	sit-ups	medium	[0.01,011]	0.01	16.91	7.97	112.3%	228.4%	648.7%
Arm	sit-ups	intense	[0.01,0.10]	0.01	19.68	10.09	95.1%	207.8%	177.2%
Arm	jogging	slow	[0.01,0.12]	0.06	4.45	1.92	131.4%	235.1%	228.6%
Arm	jogging	medium	[0.02,0.11]	0.05	9.68	4.22	129.5%	163.1%	219.6%
Arm	jogging	intense	[0.02,0.10]	0.05	7.59	3.16	140.2%	224.5%	170.6%
Leg	sit-ups	slow	[0.01,0.72]	0.35	7.07	2.95	139.8%	273.9%	258.7%
Leg	sit-ups	medium	[0.01,0.12]	0.04	8.06	6.30	27.9%	127.5%	93.7%
Leg	sit-ups	intense	[0.01,0.04]	0.04	9.53	7.42	28.4%	135.0%	225.5%
Leg	jogging	slow	[0.02,0.04]	0.02	27.39	22.41	22.2%	59.4%	53.0%
Leg	jogging	medium	[0.03,0.04]	0.03	48.83	42.74	14.2%	56.3%	38.7%
Leg	jogging	intense	[0.02,0.03]	0.03	121.30	117.64	3.1%	44.6%	20.0%
Chest	sit-ups	slow	[0.01,0.49]	0.01	20.73	7.70	169.4%	318.4%	449.0%
Chest	sit-ups	medium	[0.01,0.45]	0.01	24.27	9.15	165.3%	318.0%	961.8%
Chest	sit-ups	intense	[0.01,0.12]	0.01	27.28	11.41	139.1%	296.1%	307.2%
Chest	jogging	slow	[0.03,0.05]	0.04	3.63	3.16	14.8%	65.8%	22.2%
Chest	jogging	medium	[0.10,0.10]	0.10	0.28	0.27	3.2%	129.7%	2753.6%
Chest	jogging	intense	[0.04,0.06]	0.05	3.59	3.06	17.8%	45.3%	42.8%
Wrist	sit-ups	slow	[0.03,0.04]	0.03	3.64	2.84	28.4%	60.0%	96.7%
Wrist	sit-ups	medium	[0.02,0.09]	0.04	5.40	3.26	65.5%	112.5%	95.6%
Wrist	sit-ups	intense	[0.02,0.11]	0.03	4.84	2.81	72.3%	144.0%	83.9%
Wrist	jogging	slow	[0.01,0.12]	0.01	5.51	2.91	89.5%	197.1%	464.3%
Wrist	jogging	medium	[0.01,0.07]	0.02	25.48	17.81	43.0%	155.0%	74.7%
Wrist	jogging	intense	[0.01,0.02]	0.01	62.70	56.34	11.3%	89.4%	597.7%

Consider the average generated power under this strategy to be $P(F_{\delta}^{adp})$. The maximum average generated power can then be denoted by $P(F_{\delta^*}^{adp})$. Also, let the average generated power under optimal constant holding force be denoted by $P(F_{opt}^{c})$. In addition, consider $[\delta]^*$ to be the interval of δ in which $P(F_{\delta}^{adp}) \geq P(F_{opt}^{c})$. Define the performance improvement of the adaptive strategy compared to the optimal constant holding force strategy by the following equation.

$$PI_{F_{opt}^c}^{adp,\delta^*} = \frac{P(F_{\delta^*}^{adp}) - P(F_{opt}^{c})}{P(F_{opt}^{c})} \times 100 \tag{9}$$

Table 2 summarizes the results for acceleration measurement scenarios mentioned earlier and different adaptation intervals. The performance improvement for $[\delta]^*$ is highly dependent on the type, intensity and location of the micro-generator on the body. On average, a performance improvement of 71.7% is observed compared to the case when the optimal holding force is used. However, as explained in Remark 1, finding F_{opt}^{c} is not practical since knowledge of the entire acceleration waveform is required in advance. To gain a better sense of realistic values of the achievable performance improvement, we need to compare the average harvested power obtained using the adaptive strategy with the resulting average power using a constant (non-optimal) holding force. For example, let two constant forces F_1^c and F_2^c be chosen 50% lower and 50% higher than F_{opt}^{c}, respectively. In addition, let the performance improvement of the adaptive strategy compared to these constant holding forces be denoted by $PI_{F_1^c}^{adp,\delta^*}$ and $PI_{F_2^c}^{adp,\delta^*}$.

As observed in Table 2, a much higher performance improvement is achieved for these realistic scenarios. The average performance gain using our proposed adaptive strategy is 160.2% and 359.6% higher than when F_1^c and F_2^c are used as the constant holding forces, respectively. Similar values of performance improvements can be observed as long as the adaptation interval is chosen to be relatively small. Although we have provided information on the impact of adaptation frequency (or equivalently interval), it is conceivable that this frequency itself can also be adapted based on the intensity of human activity. This could avoid unnecessary adaptation operations, lowering energy consumption by the adaptive module and leading to an even higher gain in the harvested power. Detailed studies on the relation between the average generated power and adaptation interval are underway and will be provided in future work.

Remark 3: Building the prototype of the micro-harvester device requires additional expertise and overcoming specific practical challenges. We hope the prototype development and physical evaluation of its performance would be possible as we continue this research. In the meantime, we are optimistic about the accuracy of simulations since the fundamental physics of the CFPG operation has been carefully considered in the mathematical model.

V. CONCLUSION AND FUTURE WORK

Limited source of power is one of the major challenges in developing miniaturized medical wearable or implantable sensors with more functionality. This power is typically provided by small batteries. Integration of micro energy-harvesters with these sensors could be a promising approach to prolonging their battery lifetime. Considering the significant impact of the electrostatic force on the harvested power in a CFPG, we have proposed a simple methodology to adapt the holding force based on the input acceleration waveform. Simulation results for various human activities confirm the noticeable increase in the harvested power that can be achieved using this strategy. Other sophisticated adaptive schemes that may lead to higher output power have also been proposed for this purpose [29]. However, the complexity of such adaptive schemes is extremely important as this additional module in the CFPG architecture would itself require power to operate. This required power reduces the overall achievable gain in the harvested power compared to the case with a constant electrostatic force.

Although the computational complexity of the adaptive holding force strategy developed in this work is relatively low, further research to estimate its required power for a given adaptation interval (δ) is needed. In this paper, a fixed adaptation interval has been assumed to simplify the general optimization problem stated in Eq. (4). It is conceivable that joint holding force-adaptation interval optimization could result in higher gains. The authors plan to investigate these issues in the future.

ACKNOWLEDGMENT

The authors would like to express their gratitude to Masoud Roudneshin for conducting the human acceleration measurements and preparation of the dataset used in this paper.

REFERENCES

[1] G. E. Santagati, N. Dave, and T. Melodia, "Design and performance evaluation of an implantable ultrasonic networking platform for the Internet of Medical Things," *IEEE/ACM Trans. Netw.*, vol. 28, no. 1, pp. 29–42, Feb. 2020.

[2] Z. Xu, C. Xu, W. Liang, J. Xu, and H. Chen, "A lightweight mutual authentication and key agreement scheme for medical Internet of Things," *IEEE Access*, vol. 7, pp. 53922–53931, 2019.

[3] T. Wu, J.-M. Redouté, and M. R. Yuce, "A wireless implantable sensor design with subcutaneous energy harvesting for long-term IoT healthcare applications," *IEEE Access*, vol. 6, pp. 35801–35808, 2018.

[4] C. Beach, S. Krachunov, J. Pope, X. Fafoutis, R. J. Piechocki, I. Craddock, and A. J. Casson, "An ultra low power personalizable wrist worn ECG monitor integrated with IoT infrastructure," *IEEE Access*, vol. 6, pp. 44010–44021, 2018.

[5] M. A. Sayeed, S. P. Mohanty, E. Kougianos, and H. P. Zaveri, "eSeiz: An edge-device for accurate seizure detection for smart healthcare," *IEEE Trans. Consum. Electron.*, vol. 65, no. 3, pp. 379–387, Aug. 2019.

[6] A. Rezvanitabar, G. Jung, Y. S. Yaras, F. L. Degertekin, and M. Ghovanloo, "A power-efficient bridge readout circuit for implantable, wearable, and IoT applications," *IEEE Sensors J.*, vol. 20, no. 17, pp. 9955–9962, Sep. 2020.

[7] G.-Z. Yang, *Body Sensor Networks*. London, U.K.: Springer-Verlag, 2006.

[8] Y.-W. Chong, W. Ismail, K. Ko, and C.-Y. Lee, "Energy harvesting for wearable devices: A review," *IEEE Sensors J.*, vol. 19, no. 20, pp. 9047–9062, Oct. 2019.

[9] A. Cadei, A. Dionisi, E. Sardini, and M. Serpelloni, "Kinetic and thermal energy harvesters for implantable medical devices and biomedical autonomous sensors," *Meas. Sci. Technol.*, vol. 25, no. 1, pp. 1–14, 2013.

[10] K. Li, Q. He, J. Wang, Z. Zhou, and X. Li, "Wearable energy harvesters generating electricity from low-frequency human limb movement," *Microsyst. Nanoeng.*, vol. 4, no. 1, pp. 1–3, Sep. 2018.

[11] M. M. Sandhu, S. Khalifa, R. Jurdak, and M. Portmann, "Task scheduling for energy-harvesting-based IoT: A survey and critical analysis," *IEEE Internet Things J.*, vol. 8, no. 18, pp. 13825–13848, Sep. 2021.

[12] C. Beach and A. J. Casson, "Inertial kinetic energy harvesters for wearables: The benefits of energy harvesting at the foot," *IEEE Access*, vol. 8, pp. 208136–208148, 2020.

[13] P. Mayer, M. Magno, and L. Benini, "Energy-positive activity recognition—From kinetic energy harvesting to smart self-sustainable wearable devices," *IEEE Trans. Biomed. Circuits Syst.*, vol. 15, no. 5, pp. 926–937, Oct. 2021.

[14] M. Hassan, W. Hu, G. Lan, A. Seneviratne, S. Khalifa, and S. K. Das, "Kinetic-powered health wearables: Challenges and opportunities," *Computer*, vol. 51, no. 9, pp. 64–74, Sep. 2018.

[15] M. Cai and W.-H. Liao, "A coaxial wrist-worn energy harvester for self-powered Internet of Things sensors," *IEEE Internet Things J.*, vol. 10, no. 1, pp. 133–143, Jan. 2023.

[16] Y. Tuncel, T. Basaklar, and U. Ogras, "Wearable piezoelectric energy harvesting from human gait: Modeling and experimental validation," *IEEE Sensors J.*, vol. 22, no. 16, pp. 16617–16627, Aug. 2022.

[17] D. Ma, G. Lan, W. Xu, M. Hassan, and W. Hu, "Simultaneous energy harvesting and gait recognition using piezoelectric energy harvester," *IEEE Trans. Mobile Comput.*, vol. 21, no. 6, pp. 2198–2209, Jun. 2022.

[18] C. Bao, A. Luo, Y. Zhuang, J. Huang, and F. Wang, "A wearable health monitoring system self-powered by human-motion energy harvester," in *Proc. IEEE 16th Int. Conf. Nano/Micro Eng. Mol. Syst. (NEMS)*, Apr. 2021, pp. 990–993.

[19] K. Gandu, "Power processing for electrostatic microgenerators," Ph.D. dissertation, Imperial College, London, U.K., 2011.

[20] C. Cepnik, R. Lausecker, and U. Wallrabe, "Review on electrodynamic energy harvesters—A classification approach," *Micromachines*, vol. 4, no. 2, pp. 168–196, Apr. 2013.

[21] P. D. Mitcheson, E. M. Yeatman, G. K. Rao, A. S. Holmes, and T. C. Green, "Energy harvesting from human and machine motion for wireless electronic devices," *Proc. IEEE*, vol. 96, no. 9, pp. 1457–1486, Sep. 2008.

[22] P. D. Mitcheson, T. C. Green, E. M. Yeatman, and A. S. Holmes, "Architectures for vibration-driven micropower generators," *J. Microelectromech. Syst.*, vol. 13, no. 3, pp. 429–440, 2004.

[23] T. J. Kazmierski and S. Beeby, *Energy Harvesting Systems*. New York, NY, USA: Springer-Verlag, 2011.

[24] H. Mahboubi, K. Sayrafian, and A. G. Aghdam, "Adaptive maximization of harvested kinetic energy for small wearable medical sensors," in *Proc. IEEE Int. Conf. Commun.*, Jun. 2023, pp. 1–5.

[25] P. D. Mitcheson, "Analysis and optimisation of energy-harvesting microgenerator systems," Ph.D. dissertation, Imperial College, London, U.K., 2005.

[26] T. von Buren, P. D. Mitcheson, T. C. Green, E. M. Yeatman, A. S. Holmes, and G. Troster, "Optimization of inertial micropower generators for human walking motion," *IEEE Sensors J.*, vol. 6, no. 1, pp. 28–38, Feb. 2006.

[27] D. Budic, D. Simunic, and K. Sayrafian, "Kinetic-based micro energy-harvesting for wearable sensors," in *Proc. 6th IEEE Int. Conf. Cogn. Infocommun. (CogInfoCom)*, Oct. 2015, pp. 505–509.

[28] M. Dadfarnia, K. Sayrafian, P. Mitcheson, and J. Baras, "Maximizing output power of a CFPG micro energy-harvester for wearable medical sensors," in *Proc. 4th Int. Conf. Wireless Mobile Commun. Healthcare (MOBIHEALTH)*, 2014, pp. 218–221.

[29] M. Roudneshin, K. Sayrafian, and A. G. Aghdam, "Maximizing harvested energy in Coulomb force parametric generators," in *Proc. Amer. Control Conf. (ACC)*, Jun. 2022, pp. 1801–1807.

HAMID MAHBOUBI (Senior Member, IEEE) received the B.Sc. degree in electrical engineering from the Sharif University of Technology, Tehran, Iran, in 2003, the M.A.Sc. degree in electrical and computer engineering from the University of Tehran, Tehran, in 2006, and the Ph.D. degree from Concordia University, Montreal, QC, Canada, in 2014.

He was a Postdoctoral Fellow with the Department of Industrial Engineering and Operations Research, University of California at Berkeley, Berkeley, CA, USA. He was also a Postdoctoral Fellow with McGill University and Harvard University, from 2014 to 2017. He is currently a Senior Electrical Engineer with AECOM. His research interests include distributed robotics, the Internet of Things, networking, machine learning, cyber-physical systems, wearable sensors, smart cities, autonomous vehicles, and mobile sensor networks.

Dr. Mahboubi was a recipient of the Governor General of Canada Academic Gold Medal, in 2015. He was also a recipient of the Gold Medal from the 1999 National Math Olympiad in Iran. He was a recipient of the Natural Sciences and Engineering Research Council of Canada Postdoctoral Fellowship, the Concordia University Distinguished Doctoral Dissertation Prize in Engineering and Natural Science, the Doctoral Prize in Engineering and Computer Science, the Fonds québécois de la recherche sur la nature et les technologies Postdoctoral Award, the Bourse d'Etudes Hydro Quebec Scholarship, the Power Corporation of Canada Graduate Fellowship, and the Canadian National Award in Transportation. He was an Editorial Board Member of the IEEE SigView (IEEE Signal Processing Society), from 2014 to 2016. He was a member of the Technical Program Committee of a number of conferences, including the IEEE Global Communications Conference (GLOBECOM), IEEE Vehicular Technology Conference (VTC), European Conference on Networks and Communications (EuCNC), IEEE Conference on Control Technology and Applications (CCTA), and IEEE International Conference on Wireless for Space and Extreme Environments (WiSEE). He has served as the Chair of the Control Systems Chapter, IEEE Montreal Section, from 2012 to 2016. He is an Associate Editor of the Conference Editorial Board of the IEEE Control Systems Society.

KAMRAN SAYRAFIAN (Senior Member, IEEE) received the M.S. and Ph.D. degrees in electrical and computer engineering from Villanova University and the University of Maryland, respectively. He is currently a Senior Scientist with the Information Technology Laboratory, National Institute of Standards and Technology (NIST), Gaithersburg, MD, USA, where he leads a Strategic Program related to the application of the Internet of Things (IoT) in healthcare. He has been an affiliate Associate Professor with Concordia University, Montreal, Canada, since 2016. Before joining NIST, he was the Co-Founder of Zagros Networks, Inc., a fabless semiconductor company based in Rockville, MD, where he served as the President and a Senior Member of the Architecture Team. He has published over 120 conference and journal articles and book chapters. He is the co-inventor/inventor of four U.S. patents. His current research interests include body area networks, microenergy harvesting, automatic exposure notification, and IoT technology in healthcare. He is a fellow of the Washington Academy of Sciences. He was a recipient of the IEEE PIMRC 2009, SENSORCOMM 2011, IEEE CSCN 2018, and IEEE EuCNC 2019 Best Paper Awards. He was the Co-Chair of the Vertical Track on Health and Well-Being at the COST CA20120 "Intelligence-Enabling Radio Communications for Seamless Inclusive Interactions." He has served as the Technical Program Committee Co-Chair and the Executive Co-Chair for the IEEE PIMRC 2014 and as an organizer for several other IEEE ComSoc conferences and international workshops focused on the applications of wireless communication in healthcare. He was a major contributor to the development of the IEEE802.15.6 international standard on Body Area Networks and the recipient of the 2015 U.S. Department of Commerce Bronze Medal for his contribution to this emerging field. In 2014, he also served as the U.S. Embassy Science Fellow in Croatia. He was a member of the Editorial Board of the *IEEE Wireless Communication Magazine*, from 2016 to 2020.

AMIR G. AGHDAM (Fellow, IEEE) received the Ph.D. degree in electrical and computer engineering from the University of Toronto, Toronto, ON, Canada, in 2000. He is currently a Professor with the Department of Electrical and Computer Engineering, Concordia University, Montreal, QC, Canada, and an Associate Dean of Graduate Studies, Gina Cody School of Engineering and Computer Science. He was a Visiting Scholar with Harvard University in the fall of 2015 and was an Associate with the Harvard John A. Paulson School of Engineering and Applied Sciences, from September 2015 to December 2016. His research interests include distributed control of interconnected systems. He is a member of Professional Engineers Ontario, the Chair of the Conference Editorial Board of IEEE Control Systems Society, and the Editor-in-Chief of the IEEE SYSTEMS JOURNAL. He was a member of the Technical Program Committee of many conferences, including the IEEE Conference on Systems, Man and Cybernetics (IEEE SMC), and the IEEE Multiconference on Systems and Control (IEEE MSC). He was a member of the Review Committee for the Italian Research and University Evaluation Agency (ANVUR), from 2012 to 2013, and the Natural Sciences and Engineering Research Council of Canada (NSERC) ECE Evaluation Group, from 2014 to 2016. He was a recipient of the 2009 IEEE MGA Achievement Award. He was the 2014–2015 President of IEEE Canada and Director (Region 7), IEEE, Inc., and was also a member of the IEEE Awards Board for this period. He has also served as a member of the IEEE Medal of Honor Committee and IEEE MGA Awards and Recognition Committee. He is currently the Chair of the IEEE Medals Council. He has served as an Associate Editor for several IEEE journals, including IEEE TRANSACTIONS ON CONTROL SYSTEMS TECHNOLOGY and IEEE ACCESS.